Simple patterns for nonlinear susceptibilities near T_c

R. V. Gavai* and Sourendu Gupta†

Department of Theoretical Physics, Tata Institute of Fundamental Research, Homi Bhabha Road, Mumbai 400005, India

(Received 20 July 2005; published 12 September 2005)

Nonlinear susceptibilities up to the eighth order have been constructed in QCD with two flavors of dynamical quarks. Beyond leading order, they exhibit peaks at the crossover temperature, T_c. By analyzing their behavior in detail, we find that the dominant contributions near T_c come from a set of operators with a remarkably simple topology. Any effective theory of QCD near T_c must be able to explain these regularities.

DOI: 10.1103/PhysRevD.72.054006 PACS numbers: 12.38.Aw, 11.15.Ha, 05.70.Fh

Quark number susceptibilities (QNS) in QCD [1] are interesting because they are measurable through event-to-event fluctuations of conserved quantities in heavy-ion collisions [2]. Recent determinations of the linear QNS in lattice QCD include those in the continuum limit of the quenched theory [3], the first results in the high temperature phase of $N_f = 2$ QCD [4–6], and the first computation in $N_f = 2 + 1$ QCD [7]. The nonlinear susceptibilities (NLS) are a generalization introduced in [8,9] and have been used in finding the Taylor expansion of the pressure of the QCD plasma at finite chemical potential. The linear combinations used for pressure were also reported in $N_f = 2$ QCD [5].

Here we report on systematic simplicities of these quantities that we discovered in our investigation of QCD with light dynamical quarks. These simple patterns which we find here for the first time may be consistent with weak-coupling theory in the high temperature phase of QCD. However, in the vicinity of the finite temperature crossover at T_c, we find a different simple pattern. It seems possible to incorporate it into a simple model of the physics of the crossover. A few of these results have been discussed in [6]. Here we complete the study of the NLS started there.

The partition function for QCD at temperature T and chemical potentials μ_f for each of N_f flavors can be written in the form

$$Z(T, \{\mu_f\}) = \int \mathcal{D}U \mathrm{e}^{-S_G(T)} \prod_f \mathrm{det} M_f(m_f, T, \mu_f), \quad (1)$$

where S_G is the gluon part of the action and M denotes the Dirac operator. The pressure,

$$P(T, \{\mu_f\}) = -\frac{F}{V} = \left(\frac{T}{V}\right) \log Z(T, \{\mu_f\}), \quad (2)$$

which is a convex function of T and μ_f, can be expanded in a Taylor series about the point where all the $\mu_f = 0$ [8].

In this paper we examine staggered fermions with $N_f = 2$ and a small but nonvanishing quark mass, $m_u = m_d = m$. The Nth order derivatives in the Taylor expansion then can be taken n_u times with respect to μ_u and $n_d = N - n_u$ times with respect to μ_d. This is the nonlinear quark number susceptibility, which we write as χ_{n_u,n_d}. This new notation streamlines a more cumbersome notation which was used earlier. The translation table between these two notations can be understood from the relations—

$$\chi_{20} \equiv \chi_{uu} = \chi_{dd} \equiv \chi_{02}, \qquad \chi_{11} \equiv \chi_{ud},$$
$$\chi_{40} \equiv \chi_{uuuu} = \chi_{dddd} \equiv \chi_{04}, \qquad \chi_{22} \equiv \chi_{uudd}, \quad \text{etc.}, \quad (3)$$

where we have used flavor symmetry to write $\chi_{n_u,n_d} = \chi_{n_d,n_u}$.

The Taylor expansion of the pressure can be written as

$$\Delta P(T, \mu_u, \mu_d) \equiv P(T, \mu_u, \mu_d) - P(T, 0, 0) = \sum_{n_u,n_d} \chi_{n_u,n_d} \frac{\mu_u^{n_u}}{n_u!} \frac{\mu_d^{n_d}}{n_d!}. \quad (4)$$

The NLS above can be written down in terms of the derivatives of Z. From the expression in Eq. (1) it is clear that the derivatives with respect to the μ_f land entirely on the determinants. Now, since $\mathrm{det}M = \mathrm{exp Tr}\log M$, the first derivative gives $(\mathrm{det}M)' = \mathrm{Tr}(M^{-1}M')\,\mathrm{det}M \equiv \mathcal{O}_1\,\mathrm{det}M$. Higher derivatives can be found systematically using the additional relation $MM^{-1} = 1$, which yields $(M^{-1})' = -M^{-1}M'M^{-1}$. Our notation for operators is that $\mathcal{O}'_n = \mathcal{O}_{n+1}$, and $\mathcal{O}_{lmn\ldots} = \mathcal{O}_l\mathcal{O}_m\mathcal{O}_n\cdots$. The expectation values $\langle\mathcal{O}_{2n+1}(\mu_f = 0)\rangle = 0$ by CP symmetry. The derivatives of Z can be written in terms of expectation values of certain operators involving powers of traces of products of inverses and derivatives of the Dirac operator. Diagrammatic methods for their evaluation were developed in [8,10] and explicit expressions were written down in [6].

We report on results obtained using the configurations generated in the study reported in [6]. Details of our simulations and statistics can be found there. These results have been obtained on lattices with temporal extent $N_t = 4$, and varying N_s, with the spatial volume being large. The quark mass has been fixed in physical units to be such that $m_\pi/m_\rho = 0.31 \pm 0.01$, about 50% larger than in the real

*Electronic address: gavai@tifr.res.in
†Electronic address: sgupta@tifr.res.in

world, making this the smallest quark mass at which NLS have been studied. Details of how the temperature scale is set on the lattice also can be found in [6]. In physical units we find that the crossover temperature is $T_c/m_\rho = 0.186 \pm 0.006$.

The volume dependence of T_c has been remarked upon in [6]; we see evidence of some volume dependence in the bare coupling at the crossover, but the scale has larger uncertainties, so a finite size scaling study of the shift of T_c with V performed at these lattice cutoffs a will not be very useful. However, strong finite volume effects on the NLS were found when the spatial lattice extent was too small, $N_s < 4N_t$. In the remainder of this study, therefore, we concentrate on the NLS obtained with $N_s = 16$, using data obtained with $N_s = 24$ to make cross-checks of the results. At T_c, the finite volume shift in the results is significant, but become negligible on moving slightly away—to $0.95T_c$ or $1.05T_c$, for example.

The two leading terms in the series, the diagonal QNS, χ_{20}, and the off-diagonal QNS, χ_{11}, have been computed before. For completeness we display results from [6] in Fig. 1. Note that $\chi_{11} = (T/V)\langle \mathcal{O}_{11}\rangle$, which is a quark line disconnected diagram. Also, one can see that $\chi_{20} - \chi_{11} = (T/V)\langle \mathcal{O}_2\rangle$, which is quark line connected. Diagrammatic representations of these are shown in Fig. 2. Recall that for $T > T_c$, these diagrams have been computed in weak-coupling theory, giving reasonable agreement with the lattice results [11–13].

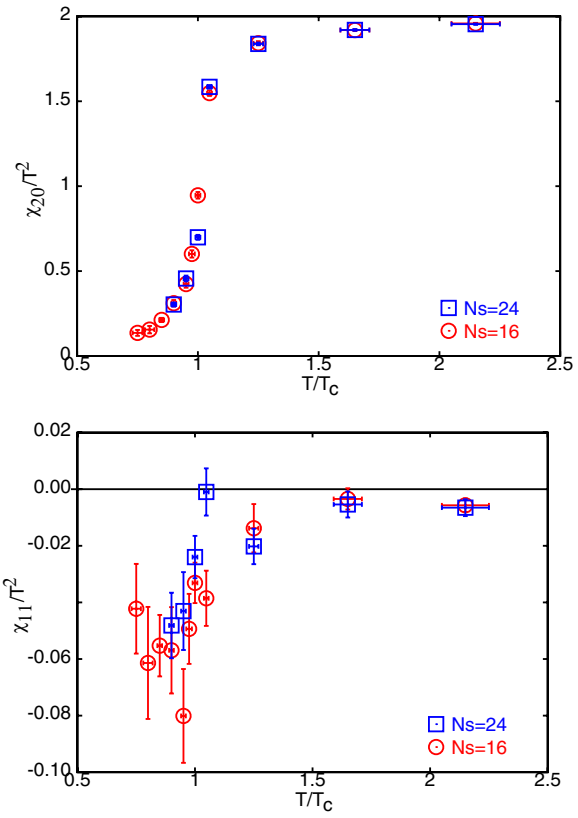

FIG. 1 (color online). χ_{20}/T^2 varies smoothly across T_c, and behaves roughly as an order parameter, being small in the hadronic phase and large in the plasma. χ_{11}/T^2 is small in the hadronic phase, perhaps peaks near T_c, and is not significant in the plasma phase. Data from lattice sizes 4×16^3 (circles) and 4×24^3 (boxes) are shown.

A counting rule for the minimum number of gluon lines needed in a quark line disconnected diagram was obtained in [11] by noting that effectively the diagrams are Abelian, and Furry's theorem holds, i.e., the number of γ_μ insertions must be even. Among these must be counted the insertions of γ_0 arising from taking derivatives with respect to the chemical potential. For $\mathcal{O}_{11}$ one gluon exchange is ruled out for reasons of gauge invariance, two by the counting rule, and hence three gluons are needed, as shown in Fig. 2.

In Fig. 1 some volume dependence is visible in the immediate vicinity of T_c. The high temperature behavior of χ_{20}/T^2 is consistent with our earlier results in [4], and, therefore, is compatible with the predictions of [11,12]. The results on χ_{11}/T^2 are also completely compatible with earlier results in [4] after correcting for a division by an extra factor of (T/V) for χ_{11}/T^2 reported there. Comparison with the recent results of [5,7] are harder to perform since the actions and quark masses are different.

At the fourth order, there are five operators—$\mathcal{O}_4$, $\mathcal{O}_{31}$, $\mathcal{O}_{22}$, $\mathcal{O}_{112}$, and $\mathcal{O}_{1111}$. The last four are quark line disconnected operators. The connected parts of the operators enter into the expressions for the NLS [6,8]. In this paper, we decompose the NLS into connected parts of these operators, such as $(T/V)\langle \mathcal{O}_{22}\rangle_c$. Since comparisons are always with connected parts, we indulge in slight notation abuse by dropping the subscript often. We remind the reader of the definitions of the connected parts at the fourth order—

$$\begin{aligned} \langle \mathcal{O}_{1111}\rangle_c &= [\langle \mathcal{O}_{1111}\rangle - 3\langle \mathcal{O}_{11}\rangle^2], \\ \langle \mathcal{O}_{112}\rangle_c &= [\langle \mathcal{O}_{112}\rangle - \langle \mathcal{O}_{11}\rangle\langle \mathcal{O}_2\rangle], \\ \langle \mathcal{O}_{22}\rangle_c &= [\langle \mathcal{O}_{22}\rangle - \langle \mathcal{O}_2\rangle^2]. \end{aligned} \tag{5}$$

$\langle \mathcal{O}_{31}\rangle$ and $\langle \mathcal{O}_4\rangle$ are connected pieces by themselves; the

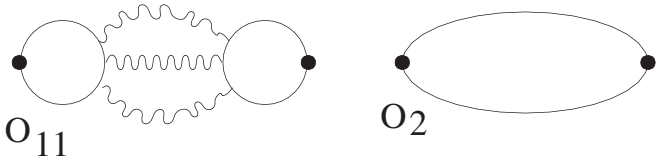

FIG. 2. The operator $\mathcal{O}_{11}$ is shown on the left with the smallest number of gluon connections between the two fermion loops. The contribution is naïvely of order g^6, but a computation shows that it is actually $g^5 \log g$ [11]. The operator $\mathcal{O}_2$ shown on the right is fermion line connected and hence the leading contribution shown is of order 1. The black dots denote insertions of γ_0 arising from the derivatives with respect to the chemical potential.

former by virtue of the fact that $\langle \mathcal{O}_n \rangle = 0$ for odd n, the latter because it is the largest loop at this order. In [6,8] we have shown that each distinct operator topology is a physical observable in a version of QCD with appropriate number of quark flavors.

We show our results for the QNS χ_{40} in Fig. 3, where we also plot the connected part of $(T/V)\langle \mathcal{O}_{22} \rangle$ multiplied by the coefficient with which it enters into χ_{40}. This operator appears to take care of the peak in the QNS near T_c. In Fig. 3 we also have shown the difference between these two quantities. The peak disappears and the remainder, in the high temperature phase, is saturated by $(T/V)\langle \mathcal{O}_4 \rangle$. Like $\mathcal{O}_2$, this expectation value is also like an order parameter, being small in the low T phase, and large on the other side of T_c.

In this range of temperatures, the two major contributions to the fourth order QNS are from $\mathcal{O}_4$ and $\mathcal{O}_{22}$. We also find this kind of peak in χ_{22}, where it again matched the peak in $(T/V)\langle \mathcal{O}_{22} \rangle$. No other QNS at this order has contribution from this operator and also shows little sign of a comparable peak near T_c. $\mathcal{O}_4$ gives no contribution to any other QNS, and, compatible with this, we see that all other

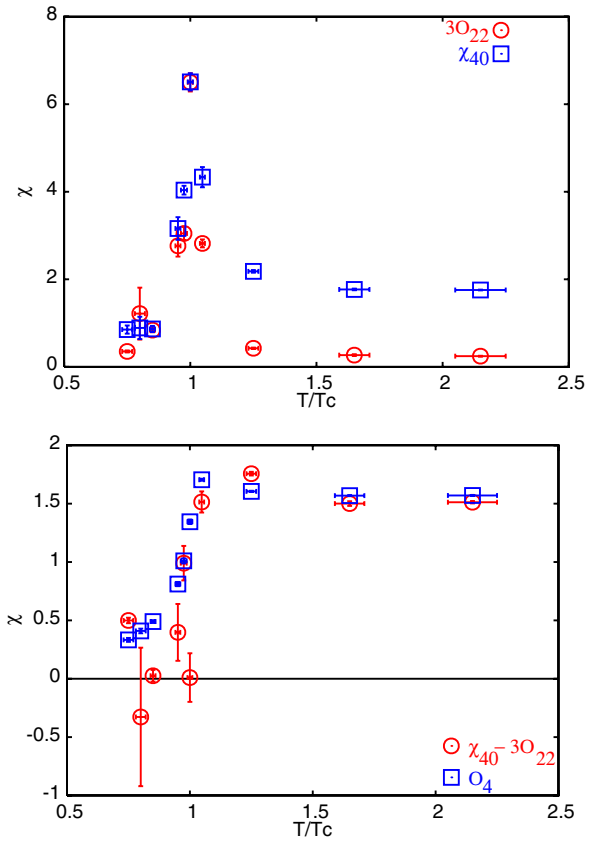

FIG. 3 (color online). χ_{40} (boxes) peaks at T_c, and the peak is entirely due to the term in $(T/V)\langle \mathcal{O}_{22} \rangle$ (circles), as shown in the lower panel. After subtracting this out, one gets a much smoother function (circles in the lower panel), which agrees well with $(T/V)\langle \mathcal{O}_4 \rangle$ (boxes). Data are from lattice sizes 4×16^3.

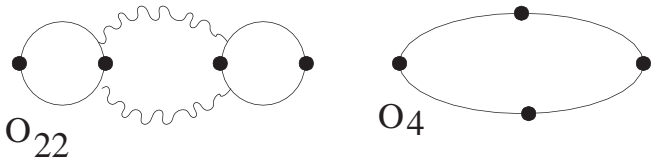

FIG. 4. One of the contributions to the operator $\mathcal{O}_{22}$ is shown on the left with the smallest number of gluon connections between the two fermion loops allowed by the counting rules of [11]. Other contributions correspond to permuting the gluon lines and operator insertions along each quark line, while keeping the loop topology fixed. The operator $\mathcal{O}_4$ shown on the right is fermion line connected and hence of order 1. These diagrams are expected to give accurate results in the plasma phase.

fourth order QNS are very small above T_c. A similar behavior is also seen on the 4×24^3 lattice.

It is interesting that the counting rules of [11] show that the two largest contributions above T_c should come from precisely these operators. $\mathcal{O}_4$ is of order 1, and the connected part of $\mathcal{O}_{22}$ shown in Fig. 4 is naïvely of order g^4. In comparison, $\mathcal{O}_{31}$ is of order g^6, $\mathcal{O}_{112}$ is of order g^8, and $\mathcal{O}_{1111}$ is of order g^{12}. These naïve powers may be modified into some logarithms in the computation.

At the sixth order we have 11 topologically distinct operators $\mathcal{O}_6$, $\mathcal{O}_{51}$, $\mathcal{O}_{42}$, $\mathcal{O}_{33}$, $\mathcal{O}_{114}$, $\mathcal{O}_{123}$, $\mathcal{O}_{222}$, $\mathcal{O}_{1113}$, $\mathcal{O}_{1122}$, $\mathcal{O}_{11\,112}$, and $\mathcal{O}_{111\,111}$. The determination of the NLS are also significantly more expensive than the linear QNS, requiring many more vectors in the stochastic evaluation of the traces [6]. One result is that the measurements are more noisy at higher orders. Nevertheless, it is possible to make significant statements about the structure of these operators.

One interesting point, illustrated in Fig. 5, is the qualitative similarity between χ_{11} and $(T/V)\langle \mathcal{O}_{33} \rangle$. Both are small in the high T phase, possibly peak in the vicinity of T_c, and are comparable to other operators in the low T phase. We have previously argued that the increase in the ratio χ_{11}/χ_{20} with decreasing T implies that the fermion

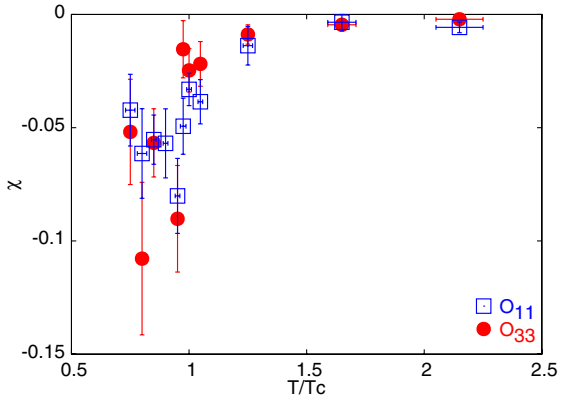

FIG. 5 (color online). χ_{11} (boxes) and $(T/V)\langle \mathcal{O}_{33} \rangle$ (circles) obtained on a 4×16^3 lattice.

sign problem becomes more severe, thus restricting the usefulness of all the recent methods which have been developed to handle this problem. The observation in Fig. 5 extends this argument to finite chemical potential.

However, at higher temperatures, such contributions are small. The dependence of χ_{60} on T is shown in Fig. 6. The peak at T_c is due to contributions from $\mathcal{O}_{222}$, as we demonstrate by plotting along with this the values of χ_{42} normalized so that the two have equal contribution from $\mathcal{O}_{222}$. The difference is small; for $T > T_c$ it is saturated by $\mathcal{O}_6$, which is much smaller than the peak, but much larger than $\mathcal{O}_{222}$. The operator $\mathcal{O}_{24}$ also peaks at T_c, but the value at the peak is negligible in comparison with $\mathcal{O}_{222}$. Power counting shows that $\mathcal{O}_6$ is of order 1, $\mathcal{O}_{24}$ is of order g^4, but $\mathcal{O}_{222}$ is of order g^6. The form of the operators is shown in Fig. 7. This is the lowest order at which we first find explicitly that the perturbative power counting of the high temperature phase does not extend down to T_c.

This pattern recurs at the eighth order, as we display in Fig. 8. There is a peak in some of the susceptibilities at T_c, but this can be ascribed to $\mathcal{O}_{2222}$. The high temperature phase is dominated by a nonvanishing value of $\mathcal{O}_8$, which is much lower than the peak. Other operators at the eighth order which may peak at T_c are $\mathcal{O}_{26}$ and $\mathcal{O}_{44}$. As we illustrate in Fig. 9, they indeed have interesting behavior near T_c. However, these operators are numerically negligible compared to the value of $\mathcal{O}_{2222}$. In the high temperature phase the power counting rules show that $\mathcal{O}_8$ is of order 1, $\mathcal{O}_{26}$ and $\mathcal{O}_{44}$ are of order g^4, whereas $\mathcal{O}_{2222}$ is of order g^8. The pattern of dominance near T_c therefore has nothing to do with power counting in g.

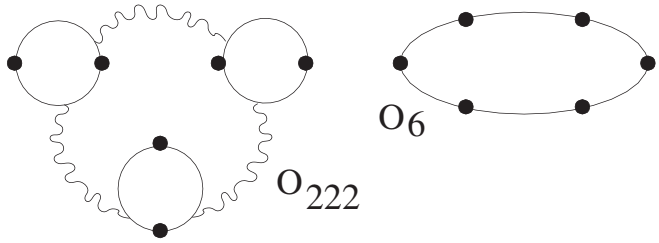

FIG. 7. One of the contributions to the operator $\mathcal{O}_{222}$ is shown on the left with the smallest number of gluon connections between the two fermion loops allowed by the counting rules of [11]. Other contributions correspond to permuting the gluon lines and operator insertions along each quark line, while keeping the loop topology fixed. The operator $\mathcal{O}_6$ shown on the right is fermion line connected and hence of order 1. These diagrams are expected to give accurate results in the plasma phase.

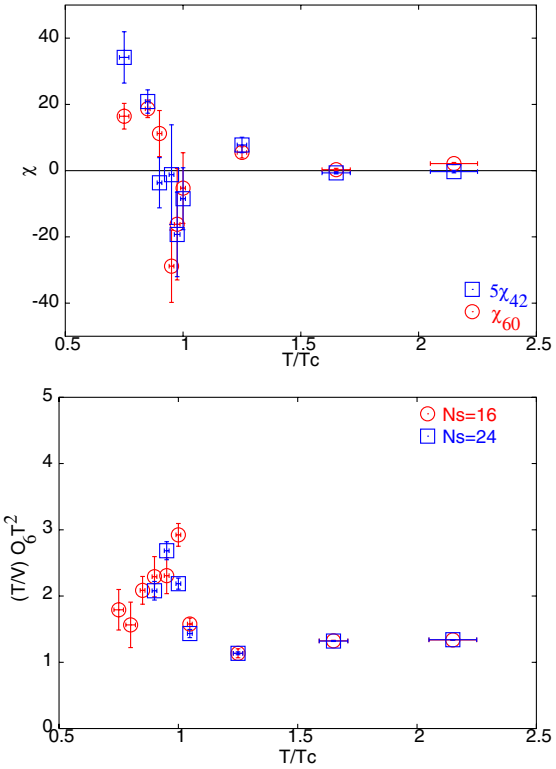

FIG. 6 (color online). In the first panel we show χ_{60} (circles) and $5\chi_{42}$ (boxes) as found on a 4×16^3 lattice. The two are normalized such that they have equal contribution from $\mathcal{O}_{222}$. The second panel shows $(T/V)\langle\mathcal{O}_6\rangle T^2$ on 4×16^3 (circles) and 4×24^3 (boxes) lattices. Note the difference in the scales of the two figures.

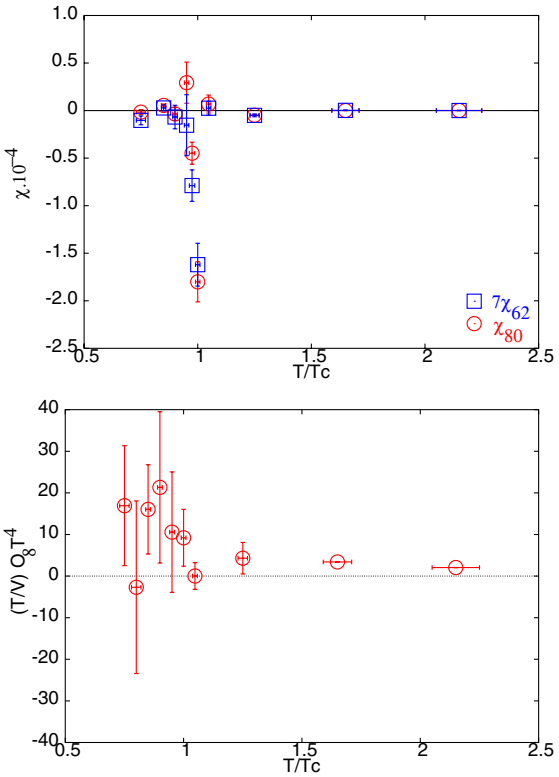

FIG. 8 (color online). In the first panel we show $\chi_{80}T^4$ (circles) and $7\chi_{62}T^4$ (boxes) as found on a 4×16^3 lattice. The two are normalized such that they have equal contribution from $\mathcal{O}_{2222}$. The second panel shows $(T/V)\langle\mathcal{O}_8\rangle T^4$ on a 4×16^3 lattice. Note the difference in the scales of the two figures.

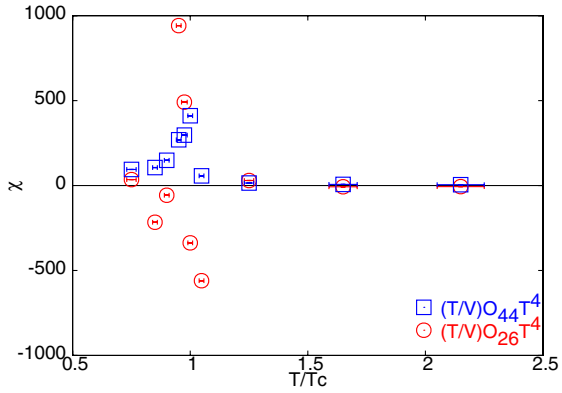

FIG. 9 (color online). The connected parts of the expectation values of $\mathcal{O}_{26}$ (circles) and $\mathcal{O}_{44}$ (boxes) as found on a 4×16^3 lattice. The expectation values are normalized by T/V and rendered dimensionless through a multiplication by T^4.

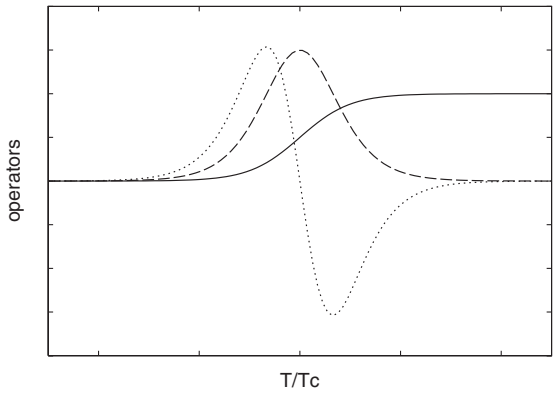

FIG. 10. The expectations for the NLS near T_c based on an effective theory of QCD near the phase transition in which the composite operator $\mathcal{O}_2$ is identified as the order parameter.

In summary then, we have found a very pleasing pattern for the NLS. In the hadronic phase, all operators seem to have comparable expectation values. This is not unexpected. In the hadronic vacuum, at $T = 0$, many different operators have vacuum expectation values, which are all typically expected to be of similar order. Above T_c, we have an extremely simple pattern, in which the NLS are dominated by the operators with a single quark loop, $\mathcal{O}_n$, and the expectation values $(T/V)\langle\mathcal{O}_n\rangle T^{n-4}$ are all in the range of 1–2. This pattern seems to be organized by weak-coupling power counting arguments, but it would be useful to have precise estimates of these operators through perturbative computations.

It follows from this observation, that the pressure at finite chemical potential has contributions from all even terms, but the numerical importance of the terms decreases factorially at high temperature. As shown in [14], in a free field theory at finite μ, the pressure can be separated into a quark piece and an antiquark piece, each of which has contributions to all even orders in μ, which cancel to give a pressure which contains only terms up to order μ^4. These small terms in the pressure can be thought of as little shifts in these pieces caused by a weak-coupling, such that the cancellation becomes incomplete. Such a mismatch between particle and antiparticle is possible because a chemical potential explicitly breaks CP invariance.

The most unexpected regularity that we have found is in the vicinity of T_c. Here, the NLS are dominated by a composite operator which is made up of appropriate numbers of fermion loops with two γ_0 insertions in each, i.e., with an appropriate number of $\mathcal{O}_2$. Our observation suggests that it may be possible to write down effective long-distance theories in which this composite bosonic operator is treated as a field operator whose expectation value shows the correct crossover behavior. In that case $\langle\mathcal{O}_{22}\rangle_c$ would be the susceptibility of this field, and being proportional to the temperature derivative of $\langle\mathcal{O}_2\rangle$, would peak, as observed. The expectation value $\langle\mathcal{O}_{222}\rangle_c$ would be proportional to the next derivative of $\langle\mathcal{O}_2\rangle$. Then the T dependence of these quantities at $\mu_f = 0$ would have the shapes shown Fig. 10.

In an effective 3D spatial Landau theory of the form that we suggest, $\mathcal{O}_2$ can be taken to be a two-point function built from one polarization of a vector operator. Under the symmetries of the transfer matrix that builds the equilibrium correlation functions, i.e., the screening correlators, this polarization mixes with the scalar [15]. It has been suggested that the scalar crucially impacts the physics of the phase transition in the chiral limit [16], because of the fact that it becomes massless at that point. This is the situation in the chiral limit; it would be interesting to see predictions from such models for the behavior of these NLS at finite quark mass.

This computation was carried out on the Indian Lattice Gauge Theory Initiative's CRAY X1 at the Tata Institute of Fundamental Research. It is a pleasure to thank Ajay Salve for his administrative support on the Cray.

[1] S. Gottlieb *et al.*, Phys. Rev. Lett. **59**, 2247 (1987).
[2] M. Asakawa, U. Heinz, and B. Muller, Phys. Rev. Lett. **85**, 2072 (2000); S.-Y. Jeon and V. Koch, Phys. Rev. Lett. **85**, 2076 (2000).
[3] R. V. Gavai and S. Gupta, Phys. Rev. D **67**, 034501 (2003).

[4] R. V. Gavai, S. Gupta, and P. Majumdar, Phys. Rev. D **65**, 054506 (2002).
[5] C. R. Allton *et al.*, Phys. Rev. D **68**, 014507 (2003).
[6] R. V. Gavai and S. Gupta, Phys. Rev. D **71**, 114014 (2005).
[7] C. Bernard *et al.*, Phys. Rev. D **71**, 034504 (2005).
[8] R. V. Gavai and S. Gupta, Phys. Rev. D **68**, 034506 (2003).
[9] R. V. Gavai and S. Gupta, Nucl. Phys. B Proc. Suppl. **129**, 524 (2004).
[10] S. Gupta, Acta Phys. Pol. B **33**, 4259 (2002).
[11] J.-P. Blaizot, E. Iancu, and A. Rebhan, Phys. Lett. B, **523**, 143 (2001).
[12] A. Vuorinen, Phys. Rev. D **68**, 054017 (2003).
[13] P. Chakraborty, M. G. Mustafa, and M. H. Thoma, Phys. Rev. D **68** 085012 (2003).
[14] S. Gupta, Phys. Lett. B **588**, 136 (2004).
[15] S. Gupta, Phys. Rev. D **60** 094505 (1999).
[16] A. Nakamura and T. Kunihiro, Phys. Rev. D **70**, 034504 (2004).